

# Intermediate-energy inverse-kinematics one-proton pickup reactions on neutron-deficient $fp$ -shell nuclei

S. McDaniel,<sup>1,2</sup> A. Gade,<sup>1,2</sup> J. A. Tostevin,<sup>3</sup> T. Baugher,<sup>1,2</sup> D. Bazin,<sup>1</sup> B. A. Brown,<sup>1,2</sup> J. M. Cook,<sup>1,2</sup> T. Glasmacher,<sup>1,2</sup> G. F. Grinyer,<sup>1,\*</sup> A. Ratkiewicz,<sup>1,2</sup> and D. Weisshaar<sup>1</sup>

<sup>1</sup>National Superconducting Cyclotron Laboratory, Michigan State University, East Lansing, Michigan 48824

<sup>2</sup>Department of Physics and Astronomy, Michigan State University, East Lansing, Michigan 48824

<sup>3</sup>Department of Physics, Faculty of Engineering and Physical Sciences, University of Surrey, Guildford, Surrey GU2 7XH, United Kingdom

(Dated: March 1, 2022)

**Background:** Thick-target-induced nucleon-adding transfer reactions onto energetic rare-isotope beams are an emerging spectroscopic tool. Their sensitivity to single-particle structure complements one-nucleon removal reaction capabilities in the quest to reveal the evolution of nuclear shell structure in very exotic nuclei. **Purpose:** To add intermediate-energy, carbon-target-induced one-proton pickup reactions to the arsenal of  $\gamma$ -ray tagged direct reactions applicable in the regime of low beam intensities and to apply these for the first time to  $fp$ -shell nuclei. **Methods:** Inclusive and partial cross sections were measured for the  $^{12}\text{C}(^{48}\text{Cr}, ^{49}\text{Mn} + \gamma)\text{X}$  and  $^{12}\text{C}(^{50}\text{Fe}, ^{51}\text{Co} + \gamma)\text{X}$  proton pickup reactions at 56.7 and 61.2 MeV/nucleon, respectively, using coincident particle- $\gamma$  spectroscopy at the NSCL. The results are compared to reaction theory calculations using  $fp$ -shell-model nuclear structure input. For comparison with our previous work, the same reactions were measured on  $^9\text{Be}$  targets. **Results:** The measured partial cross sections confirm the specific population pattern predicted by theory, with pickup into high- $\ell$  orbitals being strongly favored; driven by linear and angular momentum matching. **Conclusion:** Carbon target-induced pickup reactions are well-suited, in the regime of modest beam intensity, to study the evolution of nuclear structure, with specific sensitivities that are well described by theory.

## I. INTRODUCTION

For several decades, direct reactions have been crucial tools for the investigation of the single-particle structures that underlie the complex many-body problem of the atomic nucleus. At sufficiently high collision energies one or two nucleons can be removed from the projectile or transferred between the target and projectile nuclei in their fast, surface-grazing collisions. Classic examples of such *spectroscopic* direct reactions are light-ion-induced one- and two-nucleon transfer reactions on thin, stable targets at incident energies of several MeV per nucleon. Examples are the (d,p), (p,d), (p,t) and (t,p) reactions. Here, it is the detection of the light charged particles in the exit channel that allows the determination of final-state energies, cross sections and their angular distributions, having sensitivity to the location, spectroscopic strengths and the transferred orbital angular momenta of the active one- and two-nucleon configurations (overlaps), respectively.

With the advent of rare-isotope beam facilities, short-lived neutron-rich or neutron-deficient nuclear species have become available for nuclear structure studies. Many of the most exotic nuclei can be produced efficiently by projectile fragmentation and are available for experiments as fast heavy-ion beams with  $v/c \geq 0.30$ . In this regime, of very exotic nuclei with mod-

est beam intensities of  $1 - 10^3$  particles/second, luminosities comparable to stable-beam experiments can be restored by employing thick reaction targets and using in-beam  $\gamma$ -ray spectroscopy to tag the final states of the projectile-like reaction residues [1]. Over the past decade,  $\gamma$ -ray tagged, thick  $^9\text{Be}$  target-induced one- and two-nucleon knockout reactions in inverse kinematics, such as  $^9\text{Be}(^AZ, ^{A-1}\text{Z} + \gamma)\text{X}$  and  $^9\text{Be}(^AZ, ^{A-2}(\text{Z}-2) + \gamma)\text{X}$ , have been developed as spectroscopic reaction tools. In the low intensity, fast secondary beam regime these reaction mechanisms can probe in some detail the single-particle content of the nuclear many-body wave function at and near the Fermi surface(s) [2].

In these reactions, one-nucleon removal selectively populates hole-like configurations with respect to the projectile ground state. Similar to transfer reactions, they probe the location of such single-hole states, their spectroscopic strengths and orbital angular momenta. Sudden two-proton (neutron) removal reactions from neutron (proton)-rich nuclei also proceed as direct reactions. They probe, specifically, the parentage and phase of the participating two-nucleon configurations near the well-bound Fermi surface of the ground state of the projectile, built upon the final states of the projectile-like reaction residues [3–6]. Details of this nuclear structure model information is carried by the two-nucleon amplitudes (overlaps), see e.g. [4].

To complement this arsenal of fast-beam, inverse kinematics nucleon removal reactions, one-nucleon pickup reactions onto fast projectile beams from thick carbon and beryllium targets have recently been studied as a spectroscopic probe sensitive to *particle-like*

---

\* Present address GANIL, CEA/DSM-CNRS/IN2P3, Bvd Henri Becquerel, 14076 Caen, France

states/configurations [7–9]. The choice of reaction target is now motivated by generic linear and angular momentum matching considerations and that, at high collision energies, the pickup of well-bound target nucleons is favored [10, 11]. In common with the thick-target nucleon removal experiments, the energy resolution of the populated final-states relies on  $\gamma$ -ray spectroscopy performed in coincidence with the detection of the heavy projectile-like pickup reaction residues. However, unlike in removal reactions, and rooted in the two-body nature of the reaction mechanism, the longitudinal momentum distribution of the projectile-like reaction residues carries no useful information on the orbital angular momentum of the transferred nucleon. Rather, it can be used to estimate whether there are significant non-two-body final-state contributions to the measured reaction yields [9].

So far, thick  $^{12}\text{C}$  and  $^9\text{Be}$  targets were employed and compared [9] for the fast one-neutron pickup studies. Only  $^9\text{Be}$  targets have been used to date for measured one-proton pickup cases [7, 8]. The goals of the present work are two-fold. We investigate:

- (i) the use of a  $^{12}\text{C}$  target to induce the fast-beam one-proton pickup reaction of type  $^{12}\text{C}(^AZ, ^{A+1}(\text{Z}+1) + \gamma)$ , including the measurement and theoretical description of partial cross sections, and
- (ii) extension of the study of this spectroscopic tool into  $fp$ -shell systems.

An important aspect of the use of pickup onto fast projectile beams is the anticipated selectivity of this transfer process to high- $\ell$  orbitals, or fragments thereof, in the projectile residues, promising this technique as suited for identifying intruder states that are direct indicators of shell evolution. This makes projectiles with vacancies in the proton  $1f_{7/2}$  and  $2p_{3/2,1/2}$  orbits a logical choice to advance such one-proton pickup developments, to highlight and contrast the pickup yields into these  $\ell=3$  and  $\ell=1$  single-proton configurations.

For the present study we use a cocktail beam of projectiles containing the  $N=24$  isotones  $^{48}\text{Cr}$  and  $^{50}\text{Fe}$ . We will focus on the  $^{12}\text{C}(^{48}\text{Cr}, ^{49}\text{Mn} + \gamma)\text{X}$  and  $^{12}\text{C}(^{50}\text{Fe}, ^{51}\text{Co} + \gamma)\text{X}$  reactions at mid-target energies of 56.7 and 61.2 MeV/nucleon, respectively. To allow comparison with the earlier work (that used  $^9\text{Be}$  targets) the  $^9\text{Be}(^{48}\text{Cr}, ^{49}\text{Mn} + \gamma)\text{X}$  and  $^9\text{Be}(^{50}\text{Fe}, ^{51}\text{Co} + \gamma)\text{X}$  reactions, at mid-target energies of 50.7 and 54.8 MeV/nucleon, respectively, were also measured with the same experimental setup.

## II. EXPERIMENTS

The projectile beam containing  $^{48}\text{Cr}$  and  $^{50}\text{Fe}$  was produced by fragmentation of a 160-MeV per nucleon  $^{58}\text{Ni}$  primary beam provided by the Coupled Cyclotron Facility at the National Superconducting Cyclotron Laboratory (NSCL) at Michigan State University. The 893 mg/cm<sup>2</sup> thick  $^9\text{Be}$  production target was located at the mid-acceptance target position of NSCL's A1900

fragment separator [12]. An achromatic Al wedge of 300-mg/cm<sup>2</sup> thickness together with slit systems were used to optimize the beam purity on  $^{50}\text{Fe}$ . The resulting cocktail beam of  $N = 24$  isotones was transmitted to the reaction target position of the S800 spectrograph at typical rates of 2500, 2000, and 500 particles per second and purities of 39%, 40%, and 11%, respectively, for  $^{48}\text{Cr}$ ,  $^{49}\text{Mn}$ , and  $^{50}\text{Fe}$  at  $\Delta p/p = 1\%$  total A1900 momentum acceptance.

Reaction targets of 72.8(13)-mg/cm<sup>2</sup> thick  $^{12}\text{C}$  and 188(4)-mg/cm<sup>2</sup> thick  $^9\text{Be}$  were used at the target position of the S800 spectrograph [13] for the different settings. The high-resolution  $\gamma$ -ray detection system SeGA [14], an array of 32-fold segmented high-purity germanium detectors, was used to detect the de-excitation  $\gamma$  rays emitted by the reaction residues. Sixteen of the SeGA detectors were arranged in two rings with relative angles of 90° (9 detectors) and 37° (7 detectors) with respect to the beam axis. The high degree of segmentation allows for event-by-event Doppler reconstruction of the  $\gamma$  rays emitted by the projectile-like reaction residues in flight. The angle of the  $\gamma$ -ray emission that enters the Doppler reconstruction is deduced from the position of the segment that registered the largest  $\gamma$ -ray energy deposition. The photopeak efficiency of the detector array was calibrated with standard sources and corrected for the Lorentz boost of the  $\gamma$ -ray distribution emitted by the projectile-like reaction residues in flight at  $v/c > 0.25$ .

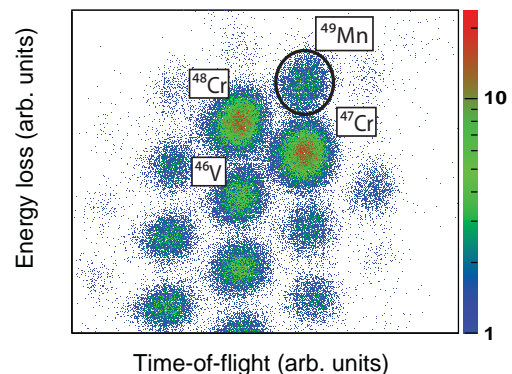


FIG. 1. (Color online) Particle identification for the reaction residues in the  $^9\text{Be}(^{48}\text{Cr}, ^{49}\text{Mn})\text{X}$  setting. Plotted is the energy loss measured with the S800 ionization chamber versus the time of flight measured between the plastic trigger scintillator at the back of the S800 focal plane and a scintillator at the spectrograph's object location.

Reaction residues were identified event-by-event with the focal-plane detection system [15] of the S800 spectrograph. The energy loss measured in the S800 ionization chamber and flight times, corrected for the angle and momentum of each nucleus, were used to identify the projectile-like reaction residues exiting the target. The incoming projectiles were identified from their difference in flight time measured with two plastic scintillators upstream of the target. The particle-identification spec-

trum for  $^{49}\text{Mn}$  produced in  $^{48}\text{Cr} + ^{12}\text{C}$  is shown in Fig. 1. The projectile beams passing through the target are close in magnetic rigidity to the respective one-proton pickup residues and the beam blocker located at the entrance of the S800 focal plane had to be used to block a large fraction of the unreacted projectiles. Still, the most intense contribution in the identification spectrum in Fig. 1 is from unreacted  $^{48}\text{Cr}$ .

For each target and projectile beam, the inclusive cross sections for the one-proton pickup reaction to all projectile + proton bound final states were deduced from the yield of detected pickup residues divided by the number of incoming projectiles relative to the number density of the  $^9\text{Be}$  and  $^{12}\text{C}$  reaction targets, respectively. The deduced inclusive cross sections are  $\sigma_{exp}^{inc}(^{49}\text{Mn}) = 2.00(13)$  mb and  $\sigma_{exp}^{inc}(^{51}\text{Co}) = 0.53(13)$  mb for the  $^{12}\text{C}$ -induced pickups and  $\sigma_{exp}^{inc}(^{49}\text{Mn}) = 1.63(8)$  mb and  $\sigma_{exp}^{inc}(^{51}\text{Co}) = 0.57(8)$  mb for the  $^9\text{Be}$ -induced pickups. The quoted uncertainties combine statistical and systematic errors, including the stability of the secondary beam composition, the choice of the software gates, and corrections for the acceptance losses in the tails of the residue parallel momentum distributions.

Event-by-event in-beam  $\gamma$ -ray spectroscopy in coincidence with detection of the projectile-like pickup residue allowed the identification of excited final states and measurement of their population in the pickup to  $^{49}\text{Mn}$ . No bound excited states were observed for  $^{51}\text{Co}$ , for which a proton separation energy of only  $S_p \approx 90$  keV is predicted from systematics [16].

Partial cross sections to individual final states were obtained from the efficiency-corrected full-energy peak areas in the Doppler reconstructed  $\gamma$ -ray spectra relative to the number of pickup products, and were corrected for feeding. Unfortunately, the statistics were not sufficient to tag the final state of the  $^{11}\text{B}$  and  $^8\text{Li}$  target residues in the laboratory-frame  $\gamma$ -ray spectra (see [7] for a higher statistics *sd*-shell case for which it was possible to tag the  $^8\text{Li}$  target residues left in the first excited state).

### III. THEORETICAL REACTION MODEL

The one-proton transfers, from  $^{12}\text{C}$  and  $^9\text{Be}$ , are assumed to take place in a single step from the ground states of these targets to bound proton single-particle states built on the ground states of the projectiles. So, as was used in earlier work, the one-proton pickup single-particle cross sections are calculated using the post-form of the distorted waves Born approximation (DWBA) to the pickup reaction transition amplitude. The transfer interaction (that binds the transferred proton and the target residues  $^{11}\text{B}$  and  $^8\text{Li}$ ) is treated in finite-range. The calculations assume that both the entrance and exit channels are two-body and hence that the proton is transferred to bound states in the projectile-like residue and the target-like residues remain bound. All calculations were performed using the direct reactions code FRESKO

[17].

The single-particle cross sections (computed for a proton + projectile spectroscopic factor of one) and the shell-model spectroscopic factors enter the calculation of the theoretical (angle integrated) pickup cross sections that are compared to the experimental results. For each final state,  $J^\pi$ , of the projectile-like residue the theoretical cross section is

$$\sigma_{th}(J^\pi) = \left( \frac{A_p}{A_p + 1} \right)^{\mathcal{N}} S_{SM}(J^\pi) \sigma_{sp}(J^\pi). \quad (1)$$

The first factor, that depends on the projectile mass  $A_p$  and the principal harmonic oscillator quantum number,  $\mathcal{N}$ , of the transferred proton orbit, is a small (near unity) center-of-mass correction to the shell-model spectroscopic factors,  $S_{SM}$ .  $\mathcal{N}=3$  for the present proton *fp*-shell cases. The measured cross sections and the calculated (single-particle) cross sections  $\sigma_{sp}(J^\pi)$  to specific final states in  $^{49}\text{Mn}$  and  $^{51}\text{Co}$  are both inclusive with respect to the final states of the target residues. The calculations thus include contributions from transitions involving several  $^{11}\text{B}$  and  $^8\text{Li}$  final states. These will be detailed in the following subsections for the  $^{12}\text{C}$  and  $^9\text{Be}$  target cases.

The spectroscopic amplitudes of the proton + projectile bound state overlaps,  $[^{48}\text{Cr}(0^+) \otimes nl_j]$  and  $[^{50}\text{Fe}(0^+) \otimes nl_j]$ , were taken from *fp*-shell-model calculations using the GXPF1A effective interaction [18]. The associated proton + projectile bound state wave functions (radial overlaps) were calculated in real Woods-Saxon potential wells with diffuseness parameter  $a_0 = 0.7$  fm and spin-orbit interaction strength of 6 MeV. The reduced radius parameters,  $r_0$ , of these potentials were adjusted to reproduce the root mean squared (rms) radii of each proton single-particle orbital given by spherical Hartree Fock calculations, as has been discussed in detail elsewhere [19]. These same Hartree-Fock (HF) calculations were used to calculate the projectile and projectile-residue densities, for calculation of the channel distorting potentials, as will be discussed below. The  $r_0$  values were 1.24 and 1.25 fm for the  $1f_{7/2}$  and  $2p$ -shell proton orbitals in  $^{49}\text{Mn}$ , respectively, and 1.23 fm for the  $1f_{7/2}$  proton orbital in  $^{51}\text{Co}$ .

#### A. Reactions on $^{12}\text{C}$ target

The proton is assumed to be transferred in a single step from a bound state in the  $^{12}\text{C}(\text{g.s.})$  into a proton + projectile bound state. The  $^{11}\text{B}$  target residue is assumed to be left in one of three bound states, the  $3/2_1^-$  ground state, the  $1/2_1^-$  excited state at 2525 keV, and the  $3/2_2^-$  excited state at 5020 keV. The shell-model spectroscopic factors (WBP effective interaction [20]) for these three states essentially exhaust the expected spectroscopic strength, of 4, being 3.16, 0.58, and 0.19, respectively. The residual strength, of 0.07, is distributed

over many states up to the proton separation energy of  $^{11}\text{B}$  and is neglected. Woods-Saxon potentials are used to generate these proton +  $^{11}\text{B}$  bound states, their geometry taken from Ref. [21]. These have reduced radius parameter  $r_0 = 1.310$  fm and diffuseness  $a = 0.55$  fm.

The nuclear distorting interactions in the  $^{12}\text{C}$  + projectile (entrance) and  $^{11}\text{B}$  + pickup residue (exit) channels were calculated. We adopted the method used in earlier fast nucleon removal reaction studies [19], i.e. by double folding the point neutron and proton densities of the projectiles and residues,  $^{48}\text{Cr}$ ,  $^{49}\text{Mn}$  and  $^{50}\text{Fe}$ ,  $^{51}\text{Co}$ , and of  $^{12}\text{C}$ ,  $^{11}\text{B}$  with an effective nucleon-nucleon ( $NN$ ) interaction [4]. For the projectile-like systems the densities were obtained from spherical Skyrme (SkX interaction) Hartree-Fock (HF) calculations [24]. The target-like systems,  $^{12}\text{C}$  and  $^{11}\text{B}$ , were assumed to have Gaussian density distributions with rms radii of 2.32 fm and 2.11 fm.

The proton pickup reactions to  $^{49}\text{Mn}$  were thus computed as  $^{48}\text{Cr}(^{12}\text{C}, ^{11}\text{B}(I^\pi))^{49}\text{Mn}(J^\pi)$  leading to the  $I^\pi = 3/2^-$ ,  $1/2^-$ , and  $3/2^-$ ,  $^{11}\text{B}$  final states. The first excited  $J^\pi = 7/2^-$ ,  $1/2^-$ , and  $3/2^-$  final states of  $^{49}\text{Mn}$  were considered. Pickup to the  $5/2^-$  ground state of  $^{49}\text{Mn}$  is negligible due to the very small shell-model spectroscopic factor,  $S_{SM} = 0.002$ . For the (as yet unobserved)  $1/2^-$  and  $3/2^-$  excited states we used the level energies of the corresponding states in the  $^{49}\text{Cr}$  mirror system. The energy of the  $7/2^-$  state is known to be 262 keV.

Table I summarizes the inputs to the reaction calculations. There,  $S_p^{\text{r.eff}} = S_p(^{49}\text{Mn}) - E_x(^{49}\text{Mn})$  is the effective proton separation energy from the projectile-like residue,  $S_p^{\text{t.eff}} = S_p(^{12}\text{C}) + E_x(^{11}\text{B})$  that from the target. The single-particle proton pickup cross section to each final state of  $^{49}\text{Mn}$  is then the sum of the cross sections to the three  $^{11}\text{B}$  final states. As expected, based on the WBP shell-model spectroscopic factors shown above, the  $^{11}\text{B}$  ground state transition dominates in these individual single-particle cross sections,  $\sigma_{sp}$ . It is already clear from Table I that our high projectile beam energy strongly favors  $\ell = 3$  pickup, to the  $1f_{7/2}$  proton state of  $^{49}\text{Mn}$ , over  $\ell = 1$  pickup to the other final states. This is understood intuitively by generic, semi-classical linear and angular momentum (mis)matching arguments, e.g. [22, 23].

Pickup to the weakly-bound dripline nucleus  $^{51}\text{Co}$  was computed similarly, as  $^{50}\text{Fe}(^{12}\text{C}, ^{11}\text{B}(I^\pi))^{51}\text{Co}$ , leading to the same  $^{11}\text{B}$  final states. Only pickup to the  $^{51}\text{Co}(7/2^-)$  ground state was considered due to the low proton separation energy of  $S_p(^{51}\text{Co}) = 90$  keV [16]. The calculations of the single-particle cross sections are summarized in Table II.

These calculated partial and summed theoretical cross sections, including the shell model spectroscopic factors and the center-of-mass corrections, are summarized in Tables V and VI. These results will be discussed and compared to the experimental data in Section IV.

TABLE I. Inputs used in the reaction model calculations for  $^{12}\text{C}(^{48}\text{Cr}, ^{49}\text{Mn})^{11}\text{B}(I^\pi)$ . Shown are the  $^{49}\text{Mn}$  final-state angular momenta and parities,  $J^\pi$ , their excitation energies,  $E_x$ , proton configurations,  $nl_j$ , and effective proton separation energies,  $S_p^{\text{r.eff}}$ . The  $^{11}\text{B}$  final-state spins and parities,  $I^\pi$ , effective proton separation energies,  $S_p^{\text{t.eff}}$ , and the single-particle cross sections,  $\sigma_{sp}$ , for each transition are also shown.

$J^\pi$	$^{49}\text{Mn}$			Target $^{12}\text{C} \rightarrow ^{11}\text{B}$		
	$E_x$ (keV)	$nl_j$	$S_p^{\text{r.eff}}$ (MeV)	$I^\pi$	$S_p^{\text{t.eff}}$ (MeV)	$\sigma_{sp}$ (mb)
$7/2^-$	262	$1f_{7/2}$	1.823	$3/2^-$	15.957	3.724
				$1/2^-$	18.082	0.238
				$3/2^-$	20.977	0.179
$1/2^-$	1703	$2p_{1/2}$	0.382	$3/2^-$	15.957	0.029
				$1/2^-$	18.082	0.010
				$3/2^-$	20.977	0.001
$3/2^-$	1741	$2p_{3/2}$	0.344	$3/2^-$	15.957	0.103
				$1/2^-$	18.082	0.008
				$3/2^-$	20.977	0.003

TABLE II. As Table I but for  $^{12}\text{C}(^{50}\text{Fe}, ^{51}\text{Co})^{11}\text{B}(I^\pi)$ .

$J^\pi$	$^{51}\text{Co}$			Target $^{12}\text{C} \rightarrow ^{11}\text{B}$		
	$E_x$ (keV)	$nl_j$	$S_p^{\text{r.eff}}$ (MeV)	$I^\pi$	$S_p^{\text{t.eff}}$ (MeV)	$\sigma_{sp}$ (mb)
$7/2^-$	0	$1f_{7/2}$	0.090	$3/2^-$	15.957	2.708
				$1/2^-$	18.082	0.165
				$3/2^-$	20.977	0.129

## B. Reactions on $^9\text{Be}$

The theoretical description of the  $^9\text{Be}$ -target-induced one-proton pickup reactions follows our earlier implementation, as was presented in [7]. In this instance two bound and one unbound final state are expected to be strongly populated in the  $^8\text{Li}$  target residue and will be considered. These are the  $2^+$  ground state, the  $1_1^+$  excited state at 980 keV, and the  $3_1^+$  state at 2255(3) keV, the latter just above the first neutron threshold of  $S_n(^8\text{Li}) = 2032.62(12)$  keV [16]. The  $^9\text{Be}(3/2^-)$  to  $^8\text{Li}(I^+)$  radial overlaps and their associated spectroscopic amplitudes used the Variational Monte Carlo (VMC) calculations of Wiringa *et al.* [25], as were discussed in Ref. [7].

As for the  $^{12}\text{C}$  target, the nuclear distorting interactions in the entrance and exit channels were obtained by double folding the point neutron and proton HF densities of the projectiles and their residues and of  $^9\text{Be}$  and  $^8\text{Li}$  with an effective  $NN$  interaction [4]. Both  $^9\text{Be}$  and  $^8\text{Li}$  were assumed to have Gaussian density distributions with an rms radius of 2.36 fm.

The pickup reaction to  $^{49}\text{Mn}$  was computed as  $^{48}\text{Cr}(^9\text{Be}, ^8\text{Li}(I^\pi))^{49}\text{Mn}(J^\pi)$  to the three final states of  $^8\text{Li}$  outlined above. The excited  $J^\pi = 7/2^-$ ,  $1/2^-$  and

TABLE III. As Table I but for  ${}^9\text{Be}({}^{48}\text{Cr}, {}^{49}\text{Mn}){}^8\text{Li}(I^\pi)$ .

$J^\pi$	${}^{49}\text{Mn}$			Target ${}^9\text{Be} \rightarrow {}^8\text{Li}$		
	$E_x$ (keV)	$n\ell_j$	$S_p^{\text{r.eff}}$ (MeV)	$I^\pi$	$S_p^{\text{t.eff}}$ (MeV)	$\sigma_{sp}$ (mb)
$7/2^-$	262	$1f_{7/2}$	1.823	$2^+$	16.888	2.213
				$1^+$	17.870	0.882
				$3^+$	19.143	0.811
$1/2^-$	1703	$2p_{1/2}$	0.382	$2^+$	16.888	0.021
				$1^+$	17.870	0.014
				$3^+$	19.143	0.004
$3/2^-$	1741	$2p_{3/2}$	0.344	$2^+$	16.888	0.049
				$1^+$	17.870	0.020
				$3^+$	19.143	0.014

TABLE IV. As Table I but for  ${}^9\text{Be}({}^{50}\text{Fe}, {}^{51}\text{Co}){}^8\text{Li}(I^\pi)$ .

$J^\pi$	${}^{51}\text{Co}$			Target ${}^9\text{Be} \rightarrow {}^8\text{Li}$		
	$E_x$ (keV)	$n\ell_j$	$S_p^{\text{r.eff}}$ (MeV)	$I^\pi$	$S_p^{\text{t.eff}}$ (MeV)	$\sigma_{sp}$ (mb)
$7/2^-$	0	$1f_{7/2}$	0.090	$2^+$	16.888	1.625
				$1^+$	17.870	0.640
				$3^+$	19.143	0.593

$3/2_1^-$   ${}^{49}\text{Mn}$  final states were considered. The input parameters and calculated cross sections are summarized in Table III, with the same entries as explained in the previous subsection. In this case the spectroscopic strengths of the different  ${}^8\text{Li}$  final states (for values, see [7]) are more equal and the ground state transition is less dominant. As previously, the one-proton pickup cross section to a particular  ${}^{49}\text{Mn}$  final state is the sum of these single-particle cross sections for the three  ${}^8\text{Li}$  final states. The calculations confirm the selectivity of pickup to the high- $\ell$  final-state configuration.

The proton pickup to  ${}^{51}\text{Co}$ , computed as  ${}^{50}\text{Fe}({}^9\text{Be}, {}^8\text{Li}(I^\pi)){}^{51}\text{Co}(7/2_{gs}^-)$  was treated similarly. The details of the calculations are summarized in Table IV.

#### IV. RESULTS AND DISCUSSION

We now discuss the experimental results from the reactions induced on the even-even  ${}^{48}\text{Cr}$  and  ${}^{50}\text{Fe}$  projectiles in comparison to the calculations presented above. We also analyze the longitudinal momentum distributions of the  ${}^{49}\text{Mn}$  and  ${}^{51}\text{Co}$  pickup residues from the reactions on the  ${}^{12}\text{C}$  target with emphasis on confirming the (assumed) two-body nature of the reaction mechanism.

#### A. Proton pickup to ${}^{49}\text{Mn}$

Neutron deficient  ${}^{49}\text{Mn}$  is well-suited to further benchmark the spectroscopic value of fast-beam one-proton pickup reactions. Having six neutrons less than the only stable Mn isotope, its low proton separation energy of  $S_p = 2085(25)$  keV [16] limits the number of proton-bound states and so minimizes the impact of possible (unobserved) indirect feeding on the determination of the partial cross sections from  $\gamma$ -ray spectroscopy. Furthermore, the proton shell structure of  ${}^{49}\text{Mn}$  allows one to examine the high- $\ell$  orbital selectivity of the pickup reaction, predicted to be strongly favored by momentum matching at high projectile energy. The yrast level scheme of  ${}^{49}\text{Mn}$ , discovered in 1970 [26], is known up to high spin values from extensive studies in the 90's focused on isospin symmetry [27, 28]. Two low-lying states, dominated by single-particle configurations involving the proton  $2p_{1/2}$  and  $2p_{3/2}$  orbits, are expected around 1700 and 1740 keV, respectively, from comparison to the mirror nucleus  ${}^{49}\text{Cr}$  [29], but have not yet been observed. The most recent work on  ${}^{49}\text{Mn}$  employed  $\beta$ -delayed proton decay from  ${}^{49}\text{Fe}$  to populate excited states in  ${}^{49}\text{Mn}$  [30].

The measured inclusive one-proton pickup reactions cross sections on the  ${}^{12}\text{C}$  and  ${}^9\text{Be}$  targets are  $\sigma_{exp}^{inc}({}^{49}\text{Mn}) = 2.00(13)$  mb and  $\sigma_{exp}^{inc}({}^{49}\text{Mn}) = 1.63(8)$  mb, respectively. These are comparable in magnitude to the earlier one-proton pickup cross section to the  $sd$ -shell nucleus  ${}^{21}\text{Na}$ , with a  ${}^9\text{Be}$  target, for which  $\sigma_{exp}^{inc} = 1.85(12)$  mb [7].

For the partial cross sections, by combining the single-particle cross sections from the reaction model calculations (Section III) with the associated GXPF1A shell-model spectroscopic factors, a distinctive population pattern is predicted from the interplay of momentum matching and proton shell structure. As can be seen from Table V, below the proton separation energy of  ${}^{49}\text{Mn}$ , only the first excited  $7/2^-$  state is predicted to be populated with appreciable cross section. Although the spectroscopic factors for pickup to the predicted  $1/2^-$  and  $3/2^-$  states (proton  $\ell = 1$ ,  $2p_{1/2}$  and  $2p_{3/2}$  configurations) are comparable to  $S_{SM}(f_{7/2})$ , the single-particle cross sections for pickup to the  $\ell = 1$  configurations are suppressed by two orders of magnitude compared to those for the  $\ell = 3$  orbital, independently of the target.

Figure 2 (upper panel) shows the Doppler-reconstructed in-beam  $\gamma$ -ray spectra detected in coincidence with  ${}^{49}\text{Mn}$ , produced in one-proton pickup from the  ${}^{12}\text{C}$  target (left) and the  ${}^9\text{Be}$  target (right). The only transition attributed to  ${}^{49}\text{Mn}$  is the de-excitation  $\gamma$ -ray from the first  $7/2^-$  to the  $5/2^-$  ground state, measured at  $E = 261$  keV. This confirms the population pattern predicted by theory with almost all cross section resulting from the pickup to the  $\ell = 3$ ,  $7/2^-$  state at 262 keV excitation energy. Within the level of the statistics, there is no evidence for the decays of the  $1/2^-$  and  $3/2^-$  excited states that are predicted to

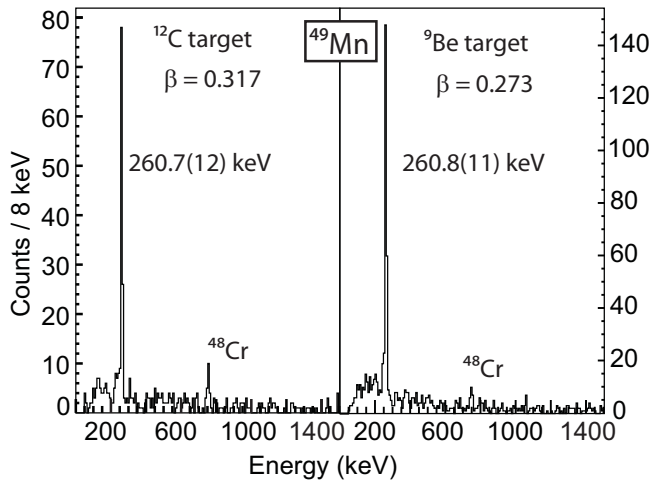


FIG. 2. Doppler-reconstructed  $\gamma$ -ray spectra in coincidence with  $^{49}\text{Mn}$  residues produced in the one-proton pickup reactions of  $^{48}\text{Cr}$  with  $^{12}\text{C}$  (left) and  $^9\text{Be}$  (right) targets. For both targets, the only prominent transition is the decay of the first excited  $7/2^-$  state to the  $5/2^-$  ground state. A peak, stemming from a tail of scattered  $^{48}\text{Cr}$  projectiles, is indicated. For the purpose of  $\gamma$ -ray spectroscopy, the software gate was generous, to include all  $^{49}\text{Mn}$  events, and therefore included a small amount of  $^{48}\text{Cr}$  scattered at large angles.

be only weakly populated in the reaction. From the efficiency-corrected peak area relative to the number of  $^{49}\text{Mn}$  produced in the pickup, the partial cross section for the population of the  $7/2^-$  state could be extracted ( $\sigma(7/2^-) = 1.60(22)$  mb for the  $^{12}\text{C}$  target and  $\sigma(7/2^-) = 1.43(15)$  mb for the  $^9\text{Be}$  target). The partial cross section to the  $^{49}\text{Mn}$  ground state was derived by subtraction, i.e.  $\sigma(g.s.) = \sigma_{exp}^{inc} - \sigma(7/2^-)$ . We note that the ground-state cross section determined in this way is an upper limit since some feeding from unobserved higher-lying proton-unbound states with a  $\gamma$ -ray branch cannot be excluded. We obtain  $\sigma(5/2_{gs}^-) \leq 0.40(25)$  mb for the  $^{12}\text{C}$ -induced reaction and  $\sigma(5/2_{gs}^-) \leq 0.20(17)$  mb for the  $^9\text{Be}$ -induced pickup. Due to the significantly reduced  $\gamma$ -ray detection efficiency at higher energies, we would not have been able to observe  $\gamma$ -ray transitions from the predicted  $1/2^-$  and  $3/2^-$  states above 1700 keV, the strongest of the two being expected to be populated at a level of less than 0.04 mb.

Figure 3 compares the measured and calculated partial cross sections for the  $^{12}\text{C}$  and  $^9\text{Be}$ -induced one-proton pickup to  $^{49}\text{Mn}$ . The measured data reproduces the distinct population pattern with almost all reactions populating the first  $7/2^-$  excited state in  $^{49}\text{Mn}$ . The measured and calculated cross sections,  $\sigma(7/2^-)$ , agree very well within the experimental uncertainty for both targets.

The measured inclusive cross section for the  $^{12}\text{C}$  target,  $\sigma_{exp}^{inc} = 2.00(13)$  mb, is about 18% higher than the calculated cross section. For the  $^9\text{Be}$  target, the measured and calculated inclusive cross sections agree, with  $\sigma_{exp}^{inc} = 1.63(8)$  mb. The measurement also confirms the

TABLE V. Shell-model proton configurations [ $^{48}\text{Cr}(0^+) \otimes n\ell_j$ ] and their spectroscopic factors,  $S_{SM}$ , single-particle cross sections to the individual final states in  $^{49}\text{Mn}$  (summed over the included  $^{11}\text{B}$  and  $^8\text{Li}$  final states), and the theoretical cross sections  $\sigma_{th}$  calculated using Eq. (1).

$J^\pi$	$E_x$ (keV)	SM conf	$S_{SM}$	$^{12}\text{C}$ target		$^9\text{Be}$ target	
				$\sigma_{sp}$ (mb)	$\sigma_{th}$ (mb)	$\sigma_{sp}$ (mb)	$\sigma_{th}$ (mb)
$7/2^-$	262	$[0^+ \otimes 1f_{7/2}]$	0.425	4.141	1.65	3.905	1.56
$1/2^-$	1703	$[0^+ \otimes 2p_{1/2}]$	0.245	0.040	0.009	0.039	0.009
$3/2^-$	1741	$[0^+ \otimes 2p_{3/2}]$	0.373	0.114	0.04	0.082	0.03
inclusive cross sections: $\sigma_{th}^{inc} = \sum_j \sigma_{th}^j$					1.70		1.60

reaction model prediction that the  $^{12}\text{C}$ -induced pickup proceeds with a slightly higher cross section.

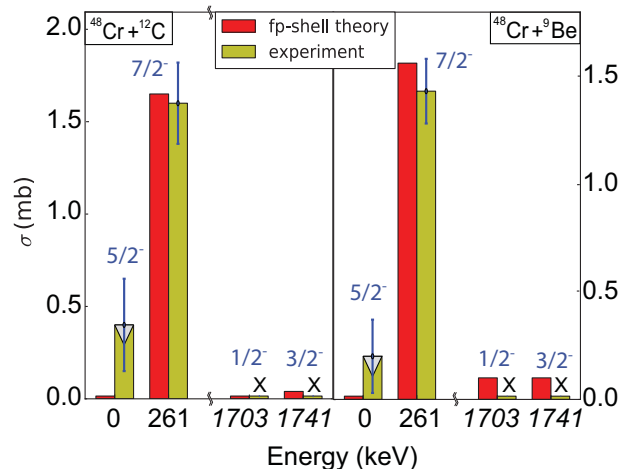


FIG. 3. (Color online) Comparison of measured and calculated partial cross sections for proton pickup to  $^{49}\text{Mn}$ . The DWBA reaction model (see text) and the shell-model spectroscopic factors from the GXPF1A effective interaction are used. The measured partial cross section to the ground state represents an upper limit obtained from the subtraction  $\sigma(g.s.) \leq \sigma_{exp}^{inc} - \sigma(7/2^-)$ . The expected higher-lying  $2p$ -shell states are predicted to be populated only very weakly and could not be observed in the present measurement (marked with x).

## B. Proton pickup to $^{51}\text{Co}$

The most neutron-deficient even- $N$  Co isotope that is known to be particle bound in its ground state,  $^{51}\text{Co}$ , was first observed in 1987 [31]. The ground state of this near-dripline nucleus was tentatively assigned to be  $7/2^-$  [29], with an evaluated proton separation energy of only  $S_p(^{51}\text{Co}) = 90$  keV based on systematics [16]. This makes  $^{51}\text{Co}$  the most weakly-bound nucleus yet studied with a fast one-nucleon pickup reaction. No

TABLE VI. As Table V but for one-proton pickup to  $^{51}\text{Co}$ .

$J^\pi$	$E_x$ (keV)	SM conf	$S_{SM}$	$^{12}\text{C}$ target		$^9\text{Be}$ target	
				$\sigma_{sp}$ (mb)	$\sigma_{th}$ (mb)	$\sigma_{sp}$ (mb)	$\sigma_{th}$ (mb)
$7/2^-$	0	$[0^+ \otimes 1f_{7/2}]$	0.246	3.002	0.70	2.858	0.66

bound or unbound excited states are reported in the literature for  $^{51}\text{Co}$ . Based on the weak binding and the non-observation of  $\gamma$ -ray transitions in coincidence with  $^{51}\text{Co}$ , we assume that, in the experiment, the cross section for the population of the ( $7/2^-$ ) ground state exhausts the inclusive cross section. This is unlike the case of the one-proton pickup from  $^{22}\text{Mg}$  to  $^{23}\text{Al}$  [8], where a  $\gamma$ -ray decay of an excited states above the proton separation energy was observed and its contribution to the transfer cross section was included in the calculations.

The measured inclusive cross sections on the  $^{12}\text{C}$  and  $^9\text{Be}$  targets are  $\sigma_{exp}^{inc}(^{51}\text{Co}) = 0.53(13)$  mb and  $\sigma_{exp}^{inc}(^{51}\text{Co}) = 0.57(8)$  mb, respectively. These are comparable in magnitude to the proton pickup cross section to the  $sd$ -shell nucleus  $^{23}\text{Al}$ , measured on a  $^9\text{Be}$  target, where  $\sigma_{exp}^{inc} = 0.54(5)$  mb [8]. We note that  $^{23}\text{Al}$  is also very weakly bound with  $S_p(^{23}\text{Al}) = 142.11(43)$  keV [32].

The weak binding of  $^{51}\text{Co}$  makes this nucleus the ideal candidate to study the one-proton pickup into the  $f_{7/2}$  orbital. As outlined above, we may assume, to a very good approximation, that  $\sigma_{exp}^{inc} = \sigma(7/2^-)$ . Table VI summarizes the shell-model spectroscopic strength for the assumed  $7/2^-$  configuration and the corresponding theoretical cross sections for the population of the  $^{51}\text{Co}$  ground state in one-proton pickup from the two targets. In spite of the weak binding and rather small spectroscopic factor,  $S_{SM} = 0.246$ , the cross section is still predicted to be of the order of 0.7 mb, which is sizable for the production of such an exotic, weakly-bound nucleus.

Figure 4 compares the measured and calculated inclusive cross sections for the ( $7/2^-$ ) ground state of  $^{51}\text{Co}$ . Measurement and the reaction model predictions agree within the experimental uncertainty for the  $^9\text{Be}$ -induced reaction while for the  $^{12}\text{C}$ -induced pickup the measurement is about 24% lower than the prediction.

### C. Momentum distribution diagnostics

In earlier work it has been pointed out that the longitudinal momentum distributions of the projectile-like one-nucleon pickup residues can be exploited as an indicator of contributions to the pickup reaction mechanism that result in non-two-body final states [9]. This diagnostic value arises since, for a strict two-body collision, the reaction-induced momentum distribution of the residues arising from kinematics and angular deflections of the reaction products is essentially  $\delta$ -function-like compared to (a) the momentum spread of the incoming beam

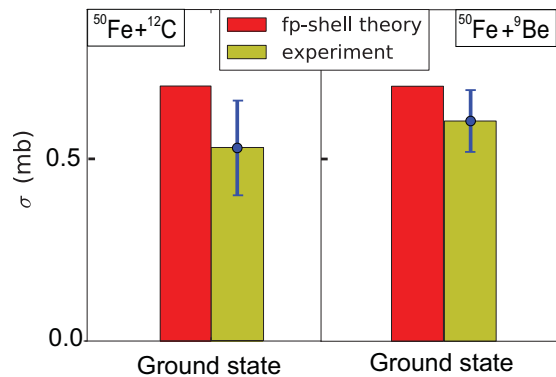


FIG. 4. (Color online) Comparison of the measured inclusive cross section and the calculated partial cross section for one-proton pickup to the ground state of  $^{51}\text{Co}$ . The DWBA reaction model (see text) and the shell-model spectroscopic factor from the GXPF1A effective interaction are used. No transitions from excited states were observed ( $S_p = 90$  keV).

of  $\Delta p/p = 1\%$  and (b) the differential momentum loss of the projectile and heavy residue in the thick target. The latter depends quite sensitively on the interaction point in the reaction target. Thus, deviations of the measured reaction residue momentum distributions from the momentum profile of the projectile beam having passed through the target and folded with the differential momentum loss of the mass ( $A_p+1$ )-residue – a rectangular function with a width that takes into account the difference in momentum of the heavy residue depending on the pickup occurring at the front or the back of the thick target – will indicate non-two-body contributions. This was demonstrated most clearly in Ref. [9], for one-neutron pickup reactions from a  $^9\text{Be}$  target, populating excited, unbound  $^8\text{Be}^*$  target residues.

Figure 5 shows the measured longitudinal momentum distributions of the  $^{49}\text{Mn}$  and  $^{51}\text{Co}$  pickup reaction residues produced on the  $^{12}\text{C}$  target. Overlaid on the figure are also (i) the momentum profiles of the unreacted  $^{48}\text{Cr}$  and  $^{50}\text{Fe}$  projectiles having passed through the target, and (ii) the result after folding these profiles with the rectangle function that takes into account the additional broadening of the distribution originating from the unknown reaction point in the (thick) reaction target.

As can be seen, after folding the projectile momentum profiles with the differential momentum loss experienced by the residues in the target, the predicted parallel momentum distributions describe the measured distributions very well. Small deviations are visible on the low-momentum side of the  $^{49}\text{Mn}$  momentum distribution where a tail structure develops. This is in line with earlier one-proton pickup reaction work on a  $^9\text{Be}$  target [7] and one-neutron pickup reaction work on  $^{12}\text{C}$  [9], where the momentum distributions show very little deviation from the strict two-body reaction mechanism expectation.

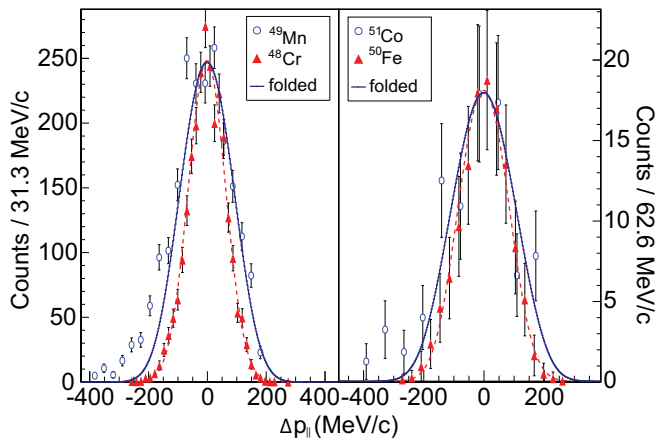


FIG. 5. (Color online) Parallel momentum distributions (blue symbols) of the  $^{49}\text{Mn}$  and  $^{51}\text{Co}$  projectile-like residues following proton pickup on a  $^{12}\text{C}$  target. For comparison, the profiles of the unreacted  $^{48}\text{Cr}$  and  $^{50}\text{Fe}$  projectiles are also shown (red symbols). The red dashed line is a fit to these data points. The solid blue line is the result of folding the projectile momentum profiles (red dashed lines) with a rectangular distribution with a width that corresponds to the differential momentum loss of the pickup reaction residues in the target, depending on the interaction point.

## V. SUMMARY AND CONCLUSION

In summary, we have employed intermediate-energy one-proton pickup reactions on  $^{12}\text{C}$  and  $^9\text{Be}$  targets to study nuclei in the  $fp$ -shell. Our experimental approach combined thick reaction targets, for luminosity, and  $\gamma$ -ray spectroscopy to tag the final states in the reaction residues. Reaction model calculations assuming one-step transfers and two-body channels were performed. Proton

pickups from  $^{48}\text{Cr}$  to  $^{49}\text{Mn}$  and from  $^{50}\text{Fe}$  to  $^{51}\text{Co}$  were studied, each on both light targets. No bound excited final states were observed in  $^{51}\text{Co}$ . The measured and calculated cross sections confirm that the  $^{51}\text{Co}$  ground state is almost certainly a  $7/2^-$  state.

The measured cross sections were found to agree well with the two-body reaction model calculations carried out in the distorted waves Born approximation. Momentum-matching considerations, embedded in the reaction model dynamics, predict a distinctive pattern of final states population in the heavy residues, with a two-order of magnitude dominance of pickup into the  $\ell = 3$ ,  $1f_{7/2}$  proton orbital compared to pickup into the  $\ell = 1$ ,  $2p_j$  orbitals. The  $^{49}\text{Mn}$  and  $^{51}\text{Co}$  longitudinal momentum distributions were also used to demonstrate that pickup events leading to non-two-body final states could make only very small contributions to the measured reaction cross sections.

The present study complements previous work, on the  $^9\text{Be}$ -induced one-proton pickup process and the  $^{12}\text{C}$ -induced one-neutron pickup reaction, and extends these studies into the  $fp$ -shell. The unique selectivity of the reaction mechanism for the population of high- $\ell$  over low- $\ell$  orbitals was clearly shown, reinforcing expectations of the potential of this reaction as a spectroscopic tool for the identification of high- $\ell$  intruder states that often indicate the breakdown of shell closures in nuclei far from stability.

## ACKNOWLEDGMENTS

This work was supported by the National Science Foundation under Grants No. PHY-0606007 and PHY-0758099 and by the UK Science and Technology Facilities Council under Grants ST/F012012/1 and ST/J000051/1. A.G. is supported by the Alfred P. Sloan Foundation.

- 
- [1] A. Gade and T. Glasmacher, *Prog. Part. Nucl. Phys.* **60**, 161 (2008).
  - [2] P. G. Hansen and J. A. Tostevin, *Annu. Rev. Nucl. Part. Sci.* **53**, 219 (2003).
  - [3] D. Bazin, B.A. Brown, C.M. Campbell, J.A. Church, D.C. Dinca, J. Enders, A. Gade, T. Glasmacher, P.G. Hansen, W.F. Mueller, H. Olliver, B.C. Perry, B.M. Sherrill, J.R. Terry, J.A. Tostevin, *Phys. Rev. Lett.* **91**, 012501 (2003).
  - [4] J. A. Tostevin, G. Podolyak, B. A. Brown, and P. G. Hansen, *Phys. Rev. C* **70**, 064602 (2004); J. A. Tostevin and B. A. Brown, *ibid.* **74**, 064604 (2006).
  - [5] K. Yoneda, A. Obertelli, A. Gade, D. Bazin, B.A. Brown, C.M. Campbell, J.M. Cook, P.D. Cottle, A.D. Davies, D.-C. Dinca, T. Glasmacher, P.G. Hansen, T. Hoagland, K.W. Kemper, J.-L. Lecouey, W.F. Mueller, R.R. Reynolds, B.T. Roeder, J.R. Terry, J.A. Tostevin, and H. Zwahlen, *Phys. Rev. C* **74**, 021303(R) (2006).
  - [6] E.C. Simpson, J.A. Tostevin, D. Bazin, B.A. Brown, and A. Gade, *Phys. Rev. Lett.* **102**, 132502 (2009).
  - [7] A. Gade, P. Adrich, D. Bazin, M.D. Bowen, B.A. Brown, C.M. Campbell, J.M. Cook, T. Glasmacher, K. Hosier, S. McDaniel, D. McGlinchery, A. Obertelli, L.A. Riley, K. Siwek, J.A. Tostevin, and D. Weisshaar, *Phys. Rev. C* **76**, 061302(R) (2007).
  - [8] A. Gade, P. Adrich, D. Bazin, M.D. Bowen, B.A. Brown, C.M. Campbell, J.M. Cook, T. Glasmacher, K. Hosier, S. McDaniel, D. McGlinchery, A. Obertelli, L.A. Riley, K. Siwek, J.A. Tostevin, D. Weisshaar, *Phys. Lett. B* **666**, 218 (2008).
  - [9] A. Gade, J. A. Tostevin, T. Baugher, D. Bazin, B. A. Brown, C. M. Campbell, T. Glasmacher, G. F. Grinyer, S. McDaniel, K. Meierbachtol, A. Ratkiewicz, S. R. Stroberg, K. A. Walsh, D. Weisshaar, and R. Winkler, *Phys. Rev. C* **83**, 054324 (2011).
  - [10] S. Shimoura, *J. Phys. G: Nucl. Part. Phys.* **31** S1759 (2005).
  - [11] S. Michimasa *et al.*, *Phys. Lett. B* **638**, 146 (2006).



- [12] D. J. Morrissey *et al.*, Nucl. Instrum. Methods in Phys. Res., Sect. B **204**, 90 (2003).
- [13] D. Bazin *et al.*, Nucl. Instrum. Methods in Phys. Res., Sect. B **204**, 629 (2003).
- [14] W. F. Mueller *et al.*, Nucl. Instr. and Methods in Phys. Res., Sect. A **466**, 492 (2001).
- [15] J. Yurkon, D. Bazin, W. Benenson, D. J. Morrissey, B. M. Sherrill, D. Swan, and R. Swanson, Nucl. Instrum. Methods in Phys. Res., Sect. A **422**, 291 (1999).
- [16] G. Audi, A.H. Wapstra, C. Thibault, Nucl. Phys. A **729**, 337 (2003).
- [17] I.J. Thompson, Computer code FRESKO. Available at <http://www.fresco.org.uk/index.htm>. See also, I.J. Thompson, Comp. Phys. Rep., **7**, 167 (1988).
- [18] M. Honma, T. Otsuka, B.A. Brown, and T. Mizusaki, Eur. Phys. J. A **25** Suppl. 1, 499 (2005).
- [19] A. Gade, P. Adrich, D. Bazin, M.D. Bowen, B.A. Brown, C.M. Campbell, J.M. Cook, T. Glasmacher, P. G. Hansen, K. Hosier, S. McDaniel, D. McGlinchery, A. Obertelli, K. Siwek, L.A. Riley, J.A. Tostevin, and D. Weisshaar, Phys. Rev. C **77**, 044306 (2008).
- [20] E. K. Warburton and B. A. Brown, Phys. Rev. C **46**, 923 (1992).
- [21] B. A. Brown, P. G. Hansen, B. M. Sherrill, and J. A. Tostevin, Phys. Rev. C **65**, 061601 (2002).
- [22] D. Brink, Phys. Lett. **B40**, 37 (1972).
- [23] W. R. Phillips, Rep. Prog. Phys. **40**, 345 (1977).
- [24] B. A. Brown, Phys. Rev. C **58**, 220 (1998).
- [25] R.W. Wiringa *et al.*, private communication. The configuration and momentum space overlaps are available at <http://www.phy.anl.gov/theory/research/overlap/>
- [26] Joseph Cerny, C.U. Cardinal, K.P. Jackson, D.K. Scott, and A.C. Shotter, Phys. Rev. Lett. **25**, 676 (1970).
- [27] C. D. O’Leary and M. A. Bentley, D. E. Appelbe, D. M. Cullen, S. Ertürk, R. A. Bark, A. Maj, and T. Saitoh, Phys. Rev. Lett. **79**, 4349 (1997).
- [28] J.A. Cameron, M.A. Bentley, A.M. Bruce, R.A. Cunningham, W. Gelletly, H.G. Price, J. Simpson, D.D. Warner, A.N. James, Phys. Lett. B **235**, 239 (1990).
- [29] National Nuclear Data Center (<http://www.nndc.bnl.gov/>).
- [30] C. Dossat, N. Adimi, F. Aksouh, F. Becker, A. Bey, B. Blank, C. Borcea, R. Borcea, A. Boston, M. Caamano, G. Chancel, M. Chartier, D. Cortina, S. Czajkowski, G. de France, F. de Oliveira Santos, A. Fleury, G. Georgiev, J. Giovinazzo, S. Grevy, R. Grzywacz, M. Hellström, M. Honma, Z. Janas, D. Karamanis, J. Kurcewicz, M. Lewitowicz, M.J. Lopez Jimenez, C. Mazzocchi, I. Matea, V. Maslov, P. Mayet, C. Moore, M. Pfützner, M.S. Pravikoff, M. Stanoiu, I. Stefan, J.C. Thomas, Nucl. Phys. A **792**, 18 (2007).
- [31] F. Pougheon, J.C. Jacmart, E. Quiniou, R. Anne, D. Bazin, V. Borrel, J. Galin, D. Guerreau, D. Guillemaud-Mueller, A.C. Mueller, E. Roeckl, M.G. Saint-Laurent, C. Detraz, Z. Phys. A **327**, 17 (1987).
- [32] A. Saastamoinen, T. Eronen, A. Jokinen, V. -V. Elomaa, J. Hakala, A. Kankainen, I. D. Moore, S. Rahaman, J. Rissanen, C. Weber, and J. Äystö, and L. Trache, Phys. Rev. C **80**, 044330 (2009).